Computation of Flow Patterns in Circulating Fluidized Beds

Flow regimes of dense-phase vertical pneumatic transport of solids, referred to in the literature as circulating fluidized beds, have been computed using a generalization of the Navier-Stokes equations for two fluids. In the less dense regime corresponding to volume fractions of solids of about 1%, the flow consists of centrally upward moving solids and downward moving clusters. The computations agree with observations made by high-speed motion pictures and with measurements of radial solids concentrations and velocities. In the dense regime, corresponding to volume fractions of about 10%, a core-annulus type of regime is obtained, with solids descending down at the wall. The computed voidage distributions and velocity profiles agree with measurement done at the Institute of Gas Technology.

Yuan P. Tsuo
MOGO Incorporated
Westmont, IL 60559

D. Gidaspow
Department of Chemical Engineering
Illinois Institute of Technology
Chicago, IL 60616

Introduction

Quantitative understanding of the hydrodynamics of circulating fluidized beds (CFB) is needed for design and scale-up of efficient new reactors in the petroleum and electric power industries. The key to a quantitative understanding of circulating fluidized beds is the prediction of the flow pattern of gas and solids in the riser. This flow pattern plays an important role in the efficiency of a CFB reactor. In the case of a combustor, the internal circulation of raw materials is an important factor in the evaluation of combustion rate since the amount of backmixing affects the residence time of gas and solids in a combustion chamber. For wall-to-bed heat transfer and thus boiler load in a CFB combustor, an understanding of particle motion is essential to achieve a good design of heat recovery (Wu et al., 1987).

Compared to the conventional bubbling bed, the CFB is characterized by high superficial gas velocities and high solid recirculation rates through the bed. Squires (1986) and Squires et al. (1985) have reviewed the subject of circulating fluidized bed applications. They call this flow regime "fast fluidization." Fast fluidization is a regime between the bubbling and the dilute-phase pneumatic transport regimes. Yerushalmi (1986) has reviewed the phenomena of fast fluidization in great depth.

In order to examine gas and solids flow patterns, a circulating fluidized bed can generally be divided into two distinct regions (Youchou and Kwauk, 1980; Weinstein et al., 1984; Matsen, 1988). In the lower part of a CFB riser there is a dense region that is considered to be a turbulent or a bubbling fluidized region. In the upper part of a CFB riser there is a dilute region that is considered as a transport region. In recent years several theoretical and experimental studies have been conducted to verify the flow patterns in CFB risers. A radial nonhomogeneous distribution of solid particles has been reported in several experimental observations (Weinstein et al., 1986; Hartge et al., 1986). Generally, the local solid volume fraction increases monotonically from the center to the wall. A core-annulus type of flow pattern in circulating fluidized beds has been shown to exist in several experimental reports (Capes and Nakamura, 1973; Gajdos and Bierl, 1978; Bader et al., 1988).

Several hydrodynamic models have been proposed to describe the axial and radial nonhomogeneous distributions of solids density in CFB risers. Rhodes and Geldart (1986) proposed a model that combines existing entrainment and bed expansion correlations with a system pressure balance to predict circulating fluidized bed hydrodynamics. They considered the dilute transport part of a CFB riser to be a long extended freeboard. They used an entrainment model to explain the observed trends in the variation of axial solids fraction profiles in the riser of a circulating fluidized bed with changes in gas velocity and solids circulation flux. They pointed out that their approach underestimated the solids concentration due to a neglect of the contribution of the downward flux at the wall. Recently, Bolton and Davidson (1988) extended Rhodes's entrainment model by taking into account a film of particle falling adjacent to the walls. They also measured the downward solids mass flux by using small protruding scoops. They concluded that the downward solids flow rate near the wall declines exponentially with height and is consistent with turbulent diffusion of entrained particles from the core to the wall.

Arastoopour and Gidaspow (1979a) modeled fast fluidization using a cluster concept and a relative velocity model (Gidaspow, 1976) in one dimension. Assuming the existence of large clusters throughout the bed, they computed the pressure drops to be in good agreement with the experiment of Yerushalmi and Squires (1977). Using the same induced-cluster concept, Horio (1988) extended the model of Nakamura and Capes (1973) for pneumatic transport to explain the high slip velocity and the annular flow of solids in fast fluidized beds.

The inhomogeneous nature of the flow has been confirmed experimentally. Therefore, the early reported high slip velocities for fast fluidized beds, by Yerushalmi et al. (1976), can be misleading due to the assumption of one-dimensional unidirectional flow. However, the formation of clusters in a circulating fluidized bed is experimentally observed in a 7.62 cm acrylic plastic tube with 520 μm glass beads and has been theoretically computed in a preliminary theoretical paper by Gidaspow et al., (1989). The clusters form near the wall, descend along the wall, and then are entrained into the core region. Similar observations and suggestions of the cluster formation have been made by others (Matsen, 1982; Grace and Tuot, 1979; Basu and Nag, 1987).

Hydrodynamic Model

The hydrodynamic model used in this study is the generalization of the inviscid model for two fluids fully reviewed by Gidaspow (1986) and previously applied to bubbling beds. It is similar to the models of Jackson (1985) and Soo (1967). To obtain a well-posed problem independent of solids stress, which is small, all the pressure drop is in the gas phase. In other words the momentum balance for the solid is just the trajectory equation for inviscid flow.

Governing equations

Table 1 shows the conservation of mass and momentum equations for each phase and the constitutive relations used. The gas and solids are treated as two interpenetrating fluids. All the solid particles are considered to be identical, characterized by a mean diameter and density. The mass and momentum balance equations for the fluidizing fluid and for the particulate phase were solved in the computer code. In these equations, the dependent variables are the void fraction, the solid volume fraction, the gas pressure, the vertical velocity components of

Table 1. Hydrodynamic Model and Constitutive Equations

Hydrodynamic Model	Constitutive Equations
Continuity Equations	**Ideal Gas Equation**
Gas phase	$\rho_g = \frac{P}{RT}$ (T6)
$\frac{\partial(\rho_g\epsilon_g)}{\partial t} + \nabla\cdot(\rho_g\epsilon_g\vec{U}_g) = 0$ (T1)	**Interphase Friction Coefficient β**
Solid phase	Based on Ergun equation
$\frac{\partial(\rho_s\epsilon_s)}{\partial t} + \nabla\cdot(\rho_s\epsilon_s\vec{U}_s) = 0$ (T2)	$\epsilon_g \le 0.8 \quad \beta = 150\frac{\epsilon_s^2\mu_g\rho_s}{(\epsilon_g d_p\phi_s)^2(\rho_s-\rho_g)} + 1.75\frac{\rho_g\rho_s\lvert U_g-U_s\rvert\epsilon_s}{(\epsilon_g d_p\phi_s)(\rho_s-\rho_g)}$ (T7)
Momentum Equations	Based on single sphere drag
Gas momentum	$\epsilon_g \ge 0.8 \quad \beta = \frac{3}{4}Cd\frac{\lvert U_g-U_s\rvert\rho_s\rho_g\epsilon_s}{d_p\phi_s(\rho_s-\rho_g)}\epsilon_g^{-2.65}$ (T8)
$\frac{\partial(\rho_g\epsilon_g\vec{U}_g)}{\partial t} + \nabla\cdot(\rho_g\epsilon_g\vec{U}_g\vec{U}_g) = -\nabla P + \beta(\vec{U}_s-\vec{U}_g) + \nabla\cdot\epsilon_g\bar{\tau}_g + \epsilon_g\rho_g g$ (T3)	with
where	$Cd = \frac{24}{Re}(1+0.15Re^{0.687}) \quad Re \le 1{,}000$
$\bar{\tau}_g = 2\mu_g\bar{D}_g - \frac{2}{3}\mu_g\nabla\cdot\vec{U}_g\bar{I}$	$Cd = 0.44 \quad Re \ge 1{,}000$
$\bar{D}_g = \frac{1}{2}[\nabla\vec{U}_g + (\nabla\vec{U}_g)^T]$	$Re = \frac{\lvert U_g-U_s\rvert d_p\rho_g\epsilon_g}{\mu_g}$
Solids momentum	**Solids Stress Modulus**
$\frac{\partial(\rho_s\epsilon_s\vec{U}_s)}{\partial t} + \nabla\cdot(\rho_s\epsilon_s\vec{U}_s\vec{U}_s) = \beta(\vec{U}_g-\vec{U}_s) - G\nabla\epsilon_s + \nabla\cdot\epsilon_s\bar{\tau}_s + \epsilon_s\rho_s g$ (T4)	$G(\epsilon_g) = \frac{\partial\tau}{\partial\epsilon_s} = 10^{-8.76\epsilon_g+5.43}\,\mathrm{N/m^2}$ (T9)
where	
$\bar{\tau}_s = 2\mu_s\bar{D}_s - \frac{2}{3}\mu_s\nabla\cdot\vec{U}_s\bar{I}$	
$\bar{D}_s = \frac{1}{2}[\nabla\vec{U}_s + (\nabla\vec{U}_s)^T]$	
$\epsilon_g + \epsilon_s = 1$ (T5)	

the gas and solids, and the horizontal velocity component of the gas and solids.

Solids viscosity

The solids viscous term is needed to account for the energy dissipation between solid particles. It arises due to the random collision of particles. The solids viscosities used were those reported by Gidaspow et al. (1989) based on measurements done at the Illinois Institute of Technology (IIT) and at the Institute of Gas Technology (IGT) in circulating fluidized beds. The viscosity coefficients, μ_s, used in the calculations were 0.509 and 0.724 Pa·s for 520 and 76 μm particles, respectively. Although the computation of viscosities by the method given by Gidaspow et al. becomes highly inaccurate when there is strong downflow of solids, and the values of some of the solids volume fractions and hence pressure losses due to solids friction may appear to be too high, the values of the solids friction coefficients obtained using these viscosities are close to those computed from the well-known (IGT, 1982) Konno-Saito (1969) correlation (see Appendix B). The solids viscosities used are also in the vicinity of those summarized by Grace (1982) for bubbling fluidized beds and used in the simulation studies by Bouillard et al (1989). In this study we considered the solids phase as a Newtonian fluid. Other rheological forms for the solids stress, such as the granular flow stress, which has a theoretical basis in dense-phase kinetic theory, have also been investigated (Ding and Gidaspow, 1990). In such an approach the solids viscosity is automatically computed from a granular flow temperature. However, the simpler approach of using an effective viscosity is used here due to difficulties encountered with granular flow theories for the more dilute flow in a CFB. For example, Sinclair and Jackson (1989) use the pipe radius as the mean free path between the particles in their granular flow theory to correct the literature value of the solids viscosity for dilute flow.

Boundary conditions and initial conditions

In this study we are only interested in the flow behavior in the riser part of a CFB. Therefore, in the computational space domain there are boundaries consisting of wall boundaries, an inflow boundary, and an outflow boundary.

Generally, for the gas and the liquid on the wall surface the flow velocities are zero in all directions. However, this is not completely true for the solid particles. Normally, when a rigid particle strikes the wall it rebounds either fully or partially. We assumed the particle to have a zero normal velocity. For the tangential direction along the wall surface the particle velocity may be between the free-slip condition and the no-slip condition. We may speculate that a fine particle may stick to the wall and a very large particle may rotate along a wall surface. Such a model has been given by Soo (1967). It is:

$$V_s\Big|_w = L_p\left(\frac{\partial V_s}{\partial r}\right)\Big|_w \qquad (1)$$

where L_p is the interaction length of particles with the fluid or the mean free path of particles.

Recently, Schnitzlein and Weinstein (1988) experimentally reported that solids loading in the fast bed is affected not only by gas velocity and solids flow rate but also by the pressure distribution in the fast bed. Therefore, the inflow gas and solid fluxes must be assigned at the inlet port. In terms of the dependent variables in governing equations, the pressure, the void fraction, and the gas and the solids velocities are assigned at the inlet boundary. One-dimensional plug flow is assumed at the inlet. For the outlet boundary, a continuation condition is applied to all dependent variables. A stationary empty pipe at ambient temperature and atmosphere pressure is used as the initial state. Appendix A shows the mathematics of the problem.

Computer code

An extension of the K-FIX computer code (Syamlal, 1985) was used to solve the governing equations. It uses the ICE method. All the simulations were done on a Cray X-MP supercomputer.

Cluster Formation Regime

A brief analysis of cluster formation has already been presented by Gidaspow et al. (1989). High-speed motion pictures showed the formation and descent of clusters for flow of 520 μm glass beads conveyed vertically upward with a gas at a velocity of 5 m/s, with a solids flux of 25 kg/m^2 s in a grounded 7.62 cm dia. acrylic plastic pipe. Figure 1 shows the geometry of the system.

Vertical pneumatic conveying has traditionally been modeled using one-dimensional equations of change (Arastoopour and Gidaspow, 1979b). The equations are those shown in Table 1, averaged over the pipe radius. This averaging procedure, described in many transport phenomena texts, introduces friction

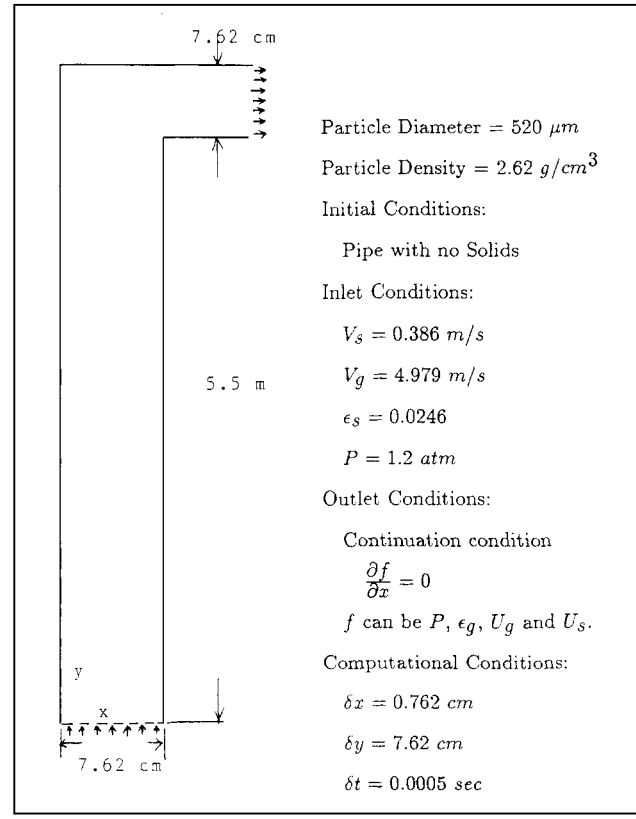

Figure 1. ITT system configuration and computational inlet conditions.

coefficients. For two-phase flow, two friction coefficients are obtained, one for the gas and one for the solid. The friction coefficients are usually (Leung, 1984) expressed in terms of Fanning's equation as

$$f_{iw} = \frac{2 f_i \epsilon \rho_i v_i^2}{D} \quad \text{where} \quad i = s, g \tag{2}$$

Here f_i is the friction factor. A modified Hagen-Poiseuille expression (Arastoopour and Gidaspow, 1979b) is used for the gas phase and Konno's correlation is used for the solid phase (Luo, 1987), as shown in Appendix B. Figure 2 shows the computed solids volume fraction vs. height at various time steps. It shows that the system reaches a steady state after a period of 5.0 s. The computed solids volume fraction in the fully developed region is 0.0065. The experimental value is 0.0115. This comparison clearly shows that one-dimensional modeling cannot be used for predicting solids concentrations. The lower computed value is due to the cluster formation, which effectively lowers the drag in a one-dimensional approximation.

A two-dimensional simulation was done for 18 s. It took a 4 s period to fully fill the empty pipe with particles. Figure 3 shows the outlet solids mass flux as a function of time. The outlet solids mass flux reached the inlet solids mass flux of 25 kg/m^2 · s at 11 s of real fluidization time. Outlet mass flux of solids oscillated at an average period of 5 s. This very low frequency of around 0.2 H is consistent with the observed and computed wall cluster descent speed of about 1 m/s. Similar speeds and low frequencies were reported by Weinstein et al. (1986) and Abed (1984) in their CFB systems.

Figure 4 shows the solids concentration profiles as a function of time. The first cluster of particles forms after 3.0 s in the center region (Tsuo, 1989). The cluster at first grew larger and denser, then it started falling down. Later several clusters formed near the wall and started to run down. A few clusters joined together and created a significant downflow. The typical wall clusters observed descend at a velocity of 1.1 m/s. The average cluster size was about 2 to 3 cm. All these phenomena

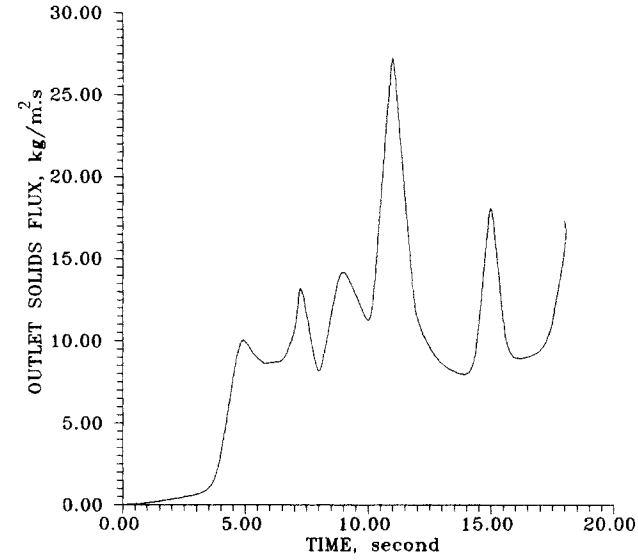

Figure 3. Computed outlet solids mass flux vs. time.

were observed in the high-speed motion pictures of the experimental run.

Initially, the gas flowed uniformly through the pipe. As the particles, dragged by the fast gas flow, came into the inlet region, the gas velocity profile assumed a nonflat shape. It formed a roughly parabolic distribution in the radial direction and had a maximum velocity at the center. The imposed velocity gradient caused by the wall pushed the particles in the radial direction. This caused cluster formation. At 2.5 s the phenomenon of first cluster formation can be seen clearly. The cluster behaves as a hydrodynamic unit or as a particle of large effective diameter. Hence it drops. Figure 4 shows the negative velocities of the clusters.

Figure 5 shows typical computed time-average and measured radial profiles of solids concentration in a developed region. Both the model and the experiment show a much higher solids

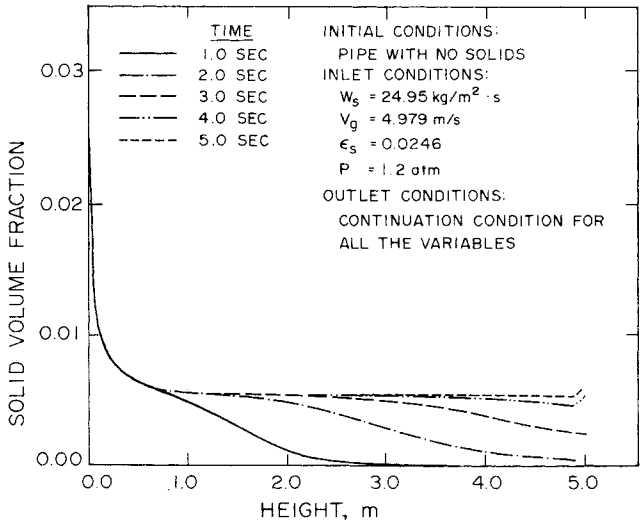

Figure 2. One-dimensional simulation of transient vertical conveying.

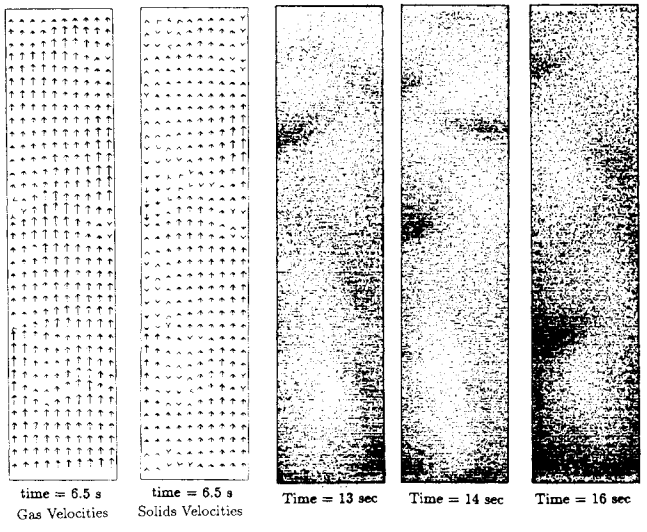

Figure 4. Computed distributions of gas velocities, solids velocities, and particle density.

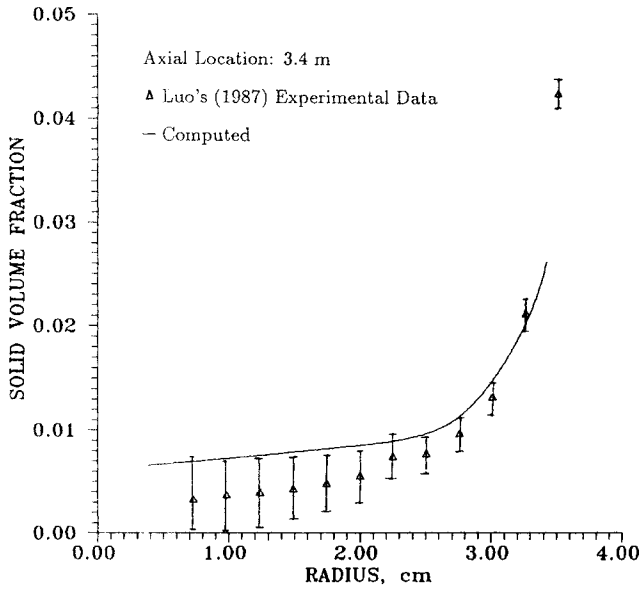

Figure 5. Radial variation of computed and measured solids volume fraction in riser.
Averaged from 10 to 15 s for computed results

concentration at the wall of the tube due to the formation of clusters near the wall.

Figure 6 shows typical computed time-average and measured radial distribution of axial solids velocities at an axial location of 3.4 m. In general, a comparison between the experimental and the computed radial distributions of axial solids velocities is good. There are some discrepancies in the center region. The solids volume fraction in the center region is around 0.005. The x-ray densitometer, which was used in Luo's (1987) experiment for measuring the solids concentration, is not considered to be accurate for such small values of solids concentration. Therefore, the experimental solids velocity, computed from the measured local flux using the ball probe and the measured local concentration, is also not accurate in the center region. Figure 7 shows typical computed time-average and measured radial distributions of axial gas velocity at an axial location of 3.4 m. A comparison between the experimental and the computed radial distributions of axial gas velocities is good.

Parametric study

Several parametric studies were conducted in order to understand the formation of clusters in CFB risers. All the results showed in this parametric study are the transient results at 6 s of real fluidization time. All the studies have the same system configuration as the previous simulation, except the study of the pipe diameter.

The effect of the superficial gas velocity was calculated at a pressure, solids mass flow rate, inlet porosity, and particle size of $P = 1.2$ atm, $W_s = 24.92\ \text{kg/m}^2 \cdot \text{s}$, $\epsilon = 0.9754$, and $D_p = 520\ \mu\text{m}$, respectively. Figure 8 shows the density plot of computed solids volume fraction for superficial gas velocities of 4.0, 5.0, and 6.0 m/s. Since the particle terminal velocity for 520 μm particle is 3.8 m/s, for the 4.0 m/s case the particles were not conveyed out the pipe but started to accumulate at the bottom. With the increase in fluidization velocity, the cluster population in the pipe decreases and the solids concentration in the pipe also decreases.

The effect of the solids circulating flow rate was calculated at a pressure, fluidization gas velocity, inlet porosity, and particle size of $P = 1.2$ atm, $U_g = 5$ m/s, $\epsilon = 0.9754$, and $D_p = 520\ \mu\text{m}$, respectively. Figure 9 shows the density plot of computed solids volume fractions at various solids circulating mass fluxes. With the decrease of the solids flow rate the cluster population in the pipe decreases and the solids concentration in the pipe also decreases. This is the expected behavior.

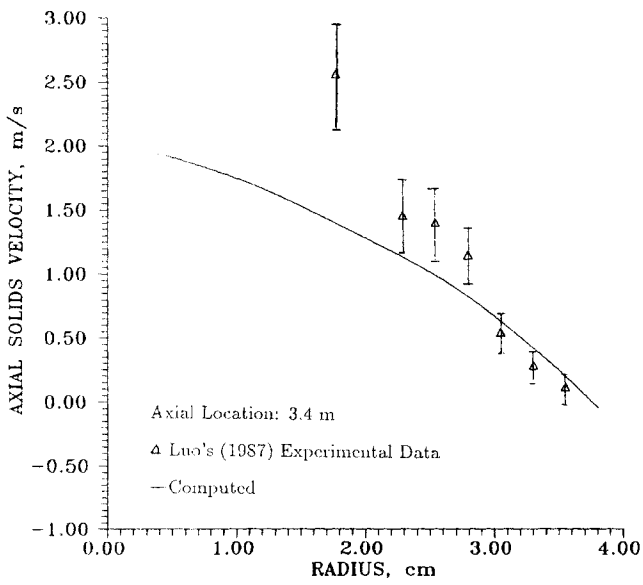

Figure 6. Radial variation of computed and measured solids velocities.
Averaged from 10 to 15 s for computed results

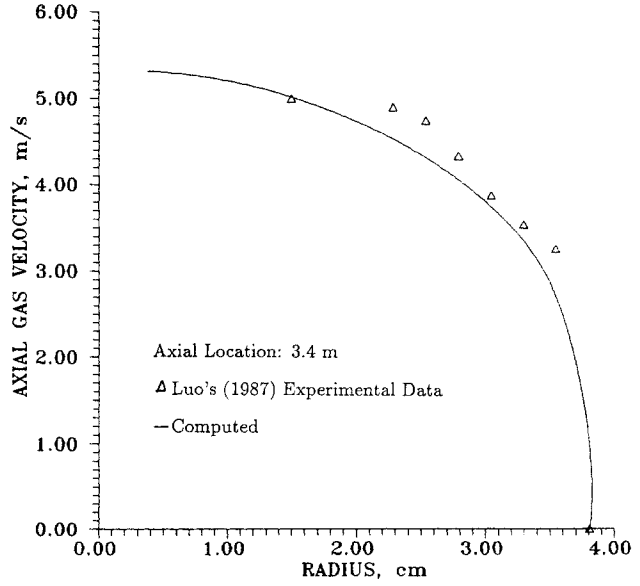

Figure 7. Radial variation of computed and measured gas velocities.
Averaged from 10 to 15 s for computed results

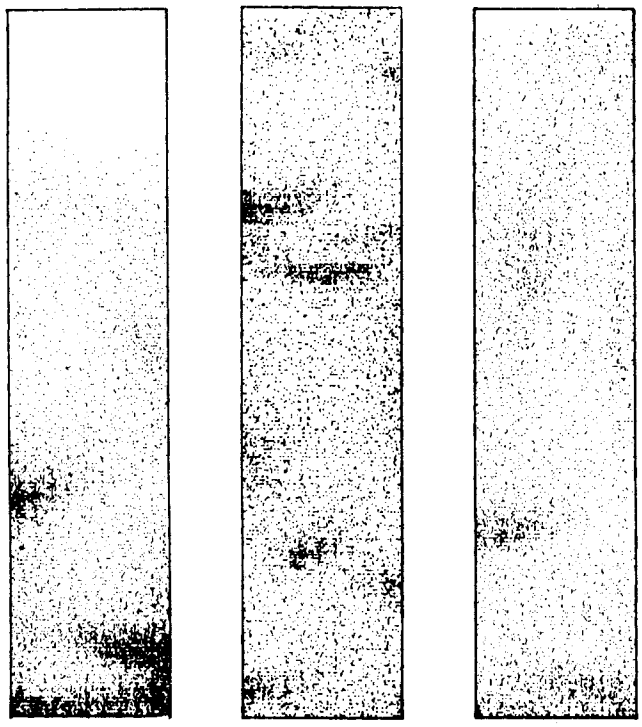

Figure 8. Effect of superficial gas velocity on cluster formation.

The effect of particle size was calculated for a pressure, fluidization gas velocity; inlet porosity, and solids mass flow rate of $P = 1.2$ atm, $U_g = 5$ m/s, $e = 0.9754$, and $W_s = 24.92$ kg/m^2 · s, respectively. Figure 10 shows the density plot of computed solids volume fractions for various particles sizes. For a particle size smaller than 300 μm, the clusters disappear. The particles move in a streamwise flow, except for a dense layer near the wall. This phenomenon may be due to a smaller terminal velocity of the smaller particles. At higher solids fluxes the clusters should reappear.

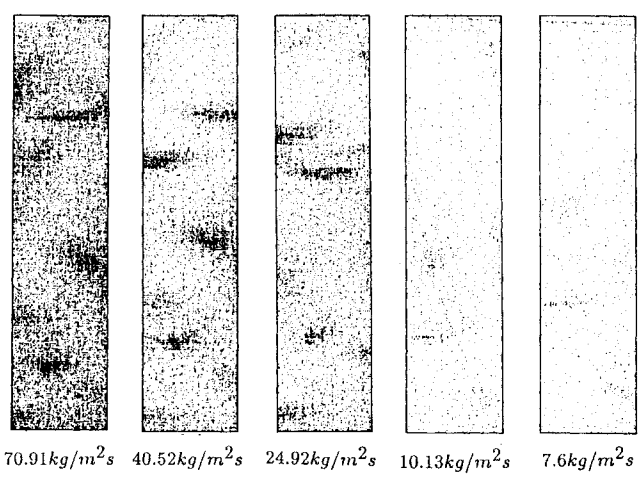

Figure 9. Effect of solids circulating flow rate on cluster formation.

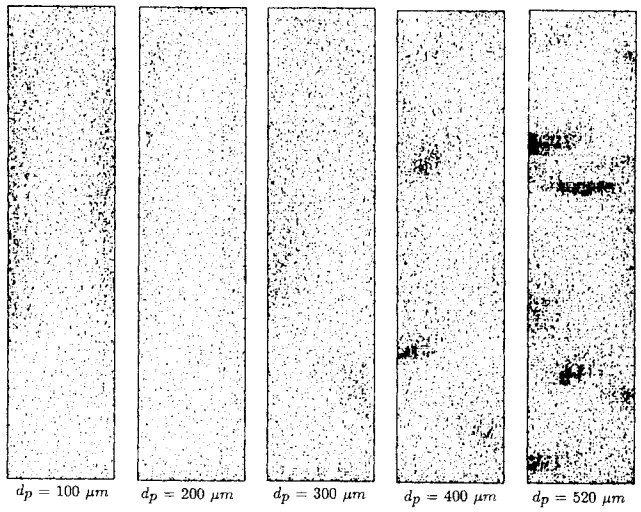

Figure 10. Effect of particle size on cluster formation.

The effect of the diameter of the pipe was calculated for a pressure, fluidization gas velocity, inlet porosity, solids mass flow rate, and particle size of $P = 1.2$ atm, $U_g = 5$ m/s, $\epsilon = 0.9574$, $W_s = 24.92$ kg/m^2 · s, and $D_p = 520$ μm, respectively. Figure 11 shows the density plot of computed solids volume fractions at two pipe diameters. As the pipe diameter increases, fewer clusters form in the pipe. This is probably due to the smaller wall surface-to-volume ratio for the larger pipe.

Core-Annulus Flow Regime

Typical dense CFB data have been obtained by Weinstein et al. (1984) at the City College of New York and by Bader et al. (1988) at the Institute of Gas Technology (IGT). The experimental conditions of Bader et al. were chosen for the computer

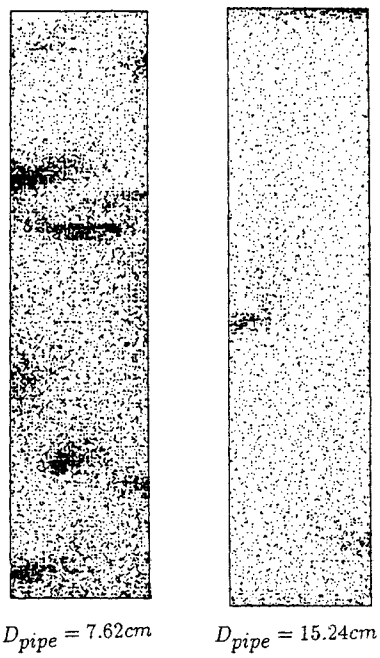

Figure 11. Effect of pipe diameter on cluster formation.

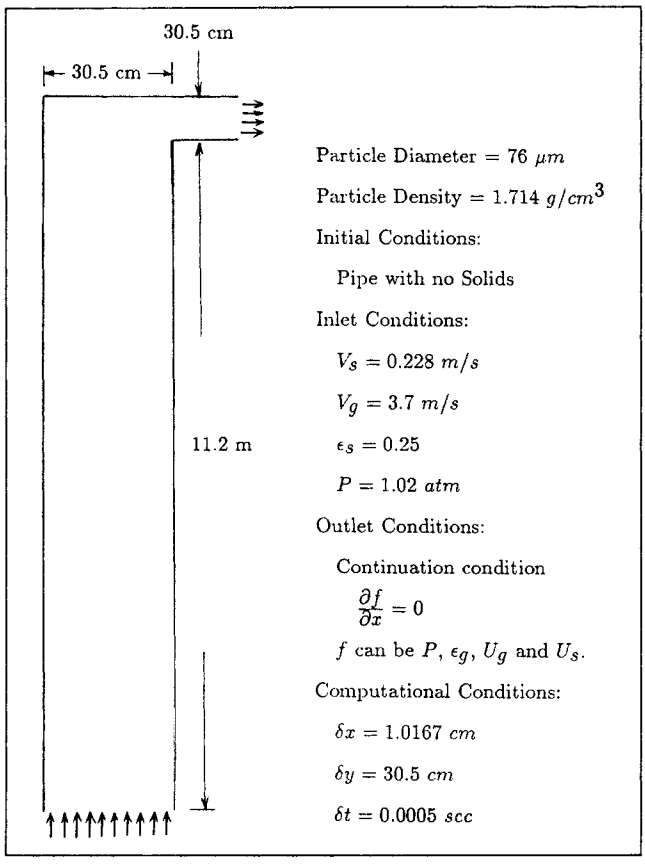

Figure 12. IGT system configuration and computational inlet conditions.

simulation. The simulations were conducted in a 30.5 cm dia. riser with 76 μm FCC catalyst. The superficial gas velocity is 3.7 m/s and the circulating solids flux is 98 kg/m^2 · s. Figure 12 shows the configuration of the system and the computational conditions.

The computer simulation was done for 18 s of the real fluidization time. It took 8 s to fully fill the empty pipe with particles. Figure 13 shows the outlet solids mass flux as the function of time. The outlet solids mass flux reached the inlet solids mass flux of 98 kg/m^2 · s at 11 s of real fluidization time. In order to obtain a reasonable time-average value for a comparison with experimental results, a 7 s computer simulation was done after the outlet solids flux reached the inlet solids flux.

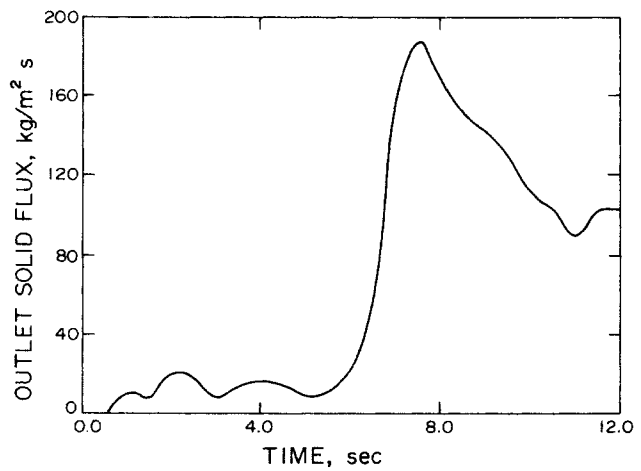

Figure 13. Computed outlet solids mass flux vs. time.

Since the solids volume fraction was directly computed in this studyy an axial profile of void fraction was obtained without interpreting it from the pressure drops, as is done in most experimental studies. Figure 14 shows a comparison of the axial porosity profiles computed by directly radially averaging them and by computing them from pressure drop equal to the weight of the bed relation. Both curves in Figure 14 show that there is a dense region at the bottom of the riser and a dilute region at the top of the riser. The directly computed porosity shows a smoothly increasing axial porosity profile along the length of the pipe and the nonexistence of a developed region. The apparent porosity, if smoothed, as experimental data would be, shows an inflection point at a height of 4 m and an approximate developed regime. This comparison shows that qualitatively different conclusions can be reached from apparent porosities and from those measured directly by radially averaging local solids volume fractions.

The computed volume fraction data were converted into a series of density plots. The number of the black dots is proportional to the volume fraction of the solid phase. Figure 15 shows the density plots for the solids volume fraction at times of 10 and 16 s after the start-up of particle injection. The empty pipe was fully filled with particles after 8 s of real fluidization time. From the dot density plots, the nonhomogeneous distribution of solid particles can be seen in both the axial and the radial directions. A dense annular layer can be seen at the wall and a dilute core can be seen at the center of the riser. Typical computed distributions of porosity in the riser at two axial locations equal to 4.1 and 9.1 m above the solids entry port are shown in Figures 16 and 17, respectively. The experimental data of Bader et al. (1988) are also included in Figures 16 and 17. A

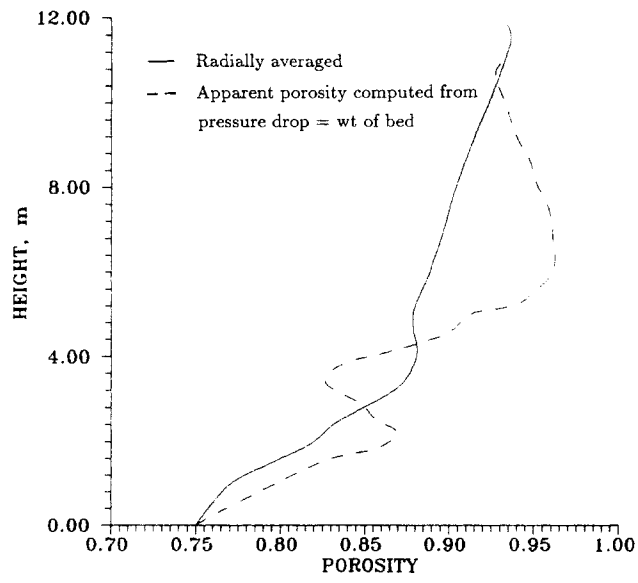

Figure 14. Computed void fractions vs. riser height for FCC at 18 s real fluidization time.

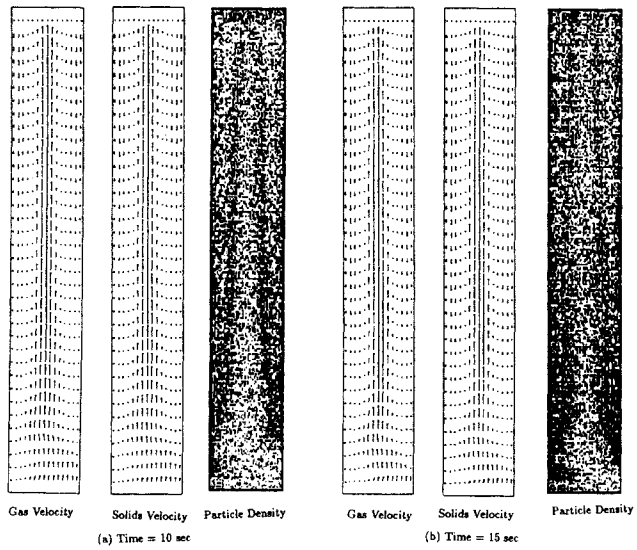

Figure 15. Computed distributions of gas velocities, solids velocities, and particle density.

comparison between the computed and the measured porosities is reasonably good. Both the theory and computation show high solids concentrations near the wall of the riser corresponding to porosities of 0.85 to 0.75, but much higher porosities, 0.95 to 0.98, at the center of the riser.

As shown in Figure 15, the flow pattern for both phases was a core-annulus type of flow. Inside the center of the pipe there is an upward, rapidly moving core surrounded by a downward, relatively slower moving annulus near the wall. Initially, the solids and the gas moved uniformly in a plug flow mode. Drag at the wall modified the flow. When the solids concentration near the wall became denser, the particles started to move downward,

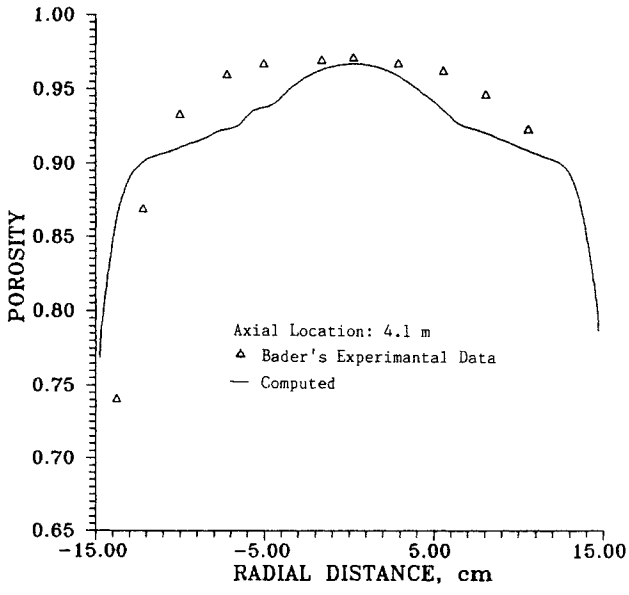

Figure 16. Radial variation of computed and measured void fraction in riser at 4.1m. Averaged from 12 to 18 s for computed results

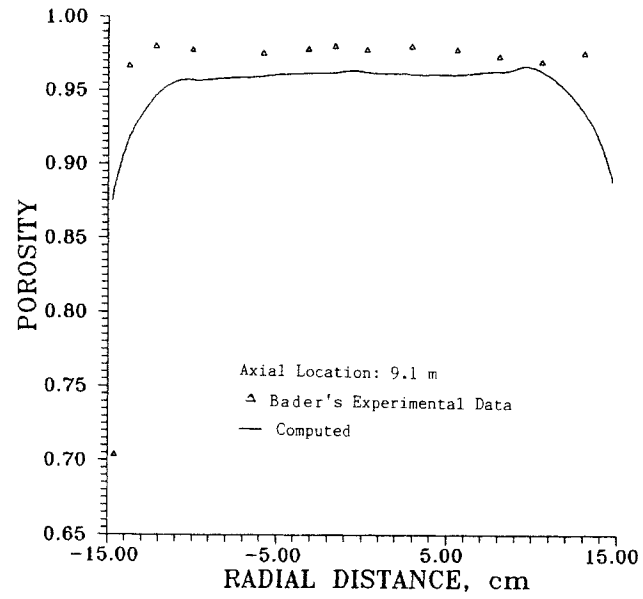

Figure 17. Radial variation of computed and measured void fraction in riser at 9.1 m.
Averaged from 12 to 18 s for computed results

due to gravitational force. Then an annular region formed near the wall. In order to conserve the inlet constant momentum, the upward velocities for both the gas and the solid phases in the core region had to increase, due to the additional area occupied by the annular region. Eventually, the upward and downward flow reached some equilibrium state.

Figures 18 and 19 show typical radial distributions of axial time-average solids velocities at axial locations of 4.1 and 9.1 m, respectively. The particle velocity in the center of the riser was computed to be two to three times the superficial gas velocity in the riser. The downcoming particle velocities near the wall at the

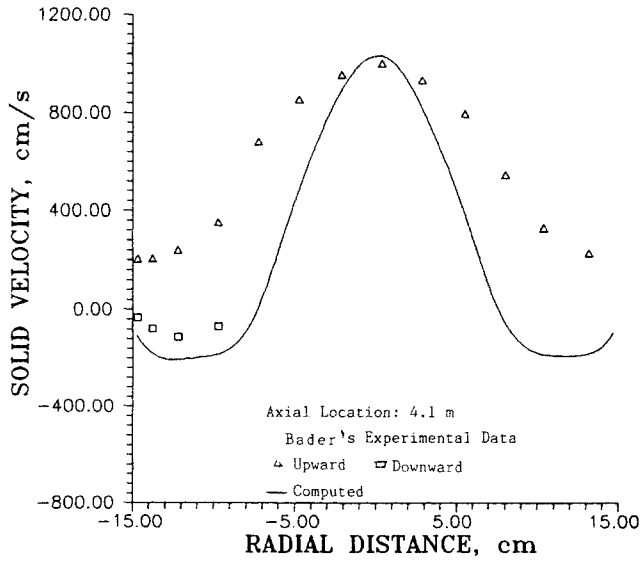

Figure 18. Radial variation of computed and measured axial solids velocity at 4.1 m.
Averaged from 12 to 18 s for computed results

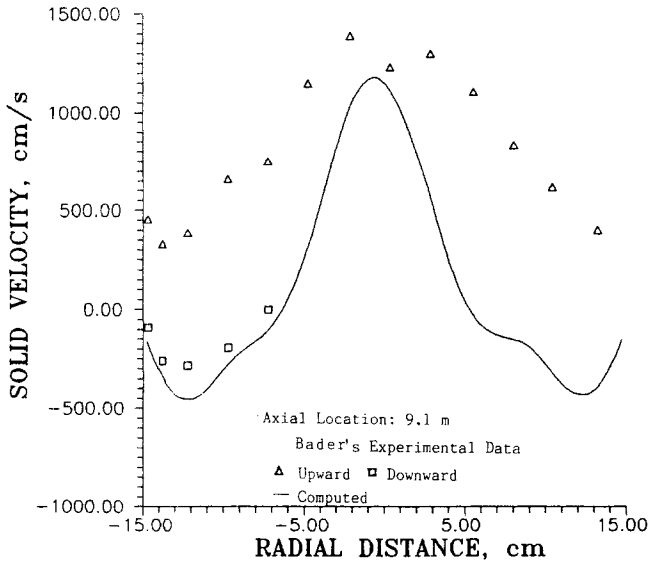

Figure 19. Radial variation of computed and measured axial solids velocity at 9.1 m.

Averaged from 10 to 18 s for computed results

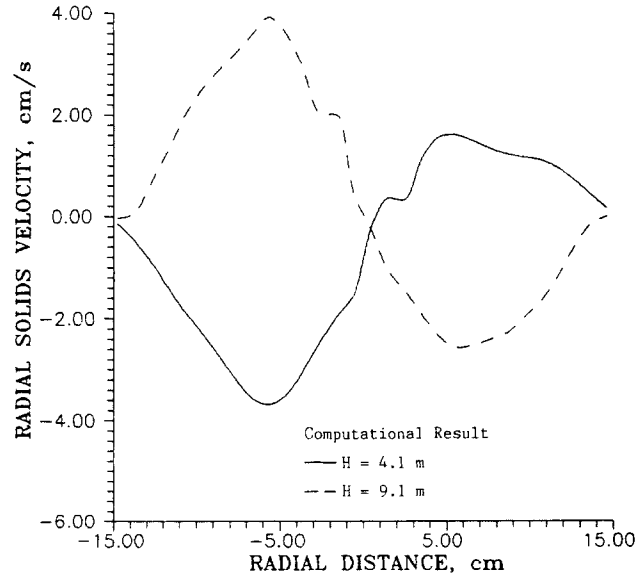

Figure 21. Radial variation of computed radial solids velocity at 15 s real fluidization time.

4.1 m level were lower than the particle velocities at the 9.1 m level in the riser. The experimental data of Bader et al. (1988) are also shown in Figures 18 and 19. In general, a comparison between the experimental and the computed radial distributions of axial solid velocities is good. There are some discrepancies in the transition region between the core and the annulus. The particles were moving slowly and locally in this transition region. The extraction sampling probe, which was used in Bader et al.'s experiment for measuring the solids flux, is not adequate in this region. Figure 20 shows typical distributions of axial gas velocity at the two locations. For 76 μm FCC particle flow the gas flow pattern is similar to the solids flow pattern.

Figure 21 shows the radial distributions of radial solids velocities at 15 s of real fluidization time at the two locations of 4.1 and 9.1 m. The particles at the 4.1 m level moved from the wall to the center and at the 9.1 m level moved in the reverse direction, from the center to the wall. Therefore, axial backmixing existed inside the riser. Since the radial particle velocities were relatively small, 1 to 10 cm/s, axial backmixing was small relative to the convective bulk flow, with high upward velocities of 10 to 15 m/s in the core region of the riser.

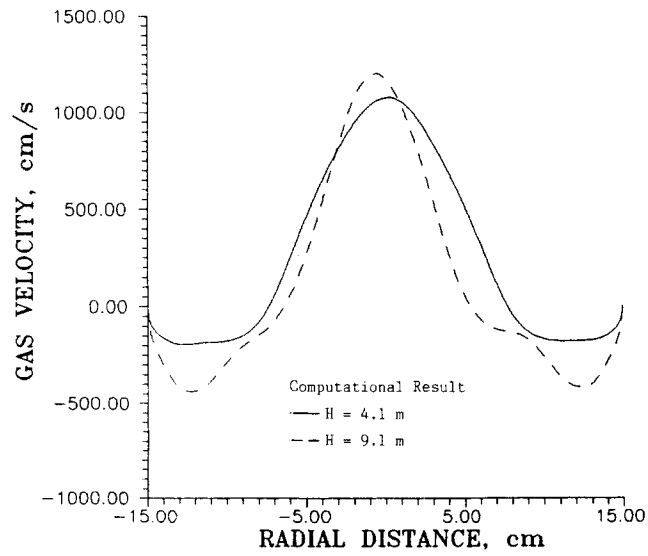

Figure 20. Radial variation of axial gas velocity.

Averaged from 12 to 18 s for computed results

Conclusions

1. A generalization of the Navier-Stokes equations for two fluids, with a solids viscosity determined from riser experiments, is capable of predicting flow regimes in circulating fluidized beds.

2. In the dilute circulating fluidized bed regime the model predicts cluster formations, in agreement with observation. These wall clusters descend at the wall, while the solids are transported up in the center of the vessel. The model predicts reasonable dependence on solids flux, gas velocity, particle size, and pipe diameter.

3. In the dense circulating fluidized bed regime the model predicts a core-annulus type of flow. The particles are transported up rapidly in the center of core. They descend slowly at the walls of the pipe. The computed radial solids velocity and particle concentration profiles agree with the measurements done at IGT. The only experimental input into the model was the solids viscosity.

4. One-dimensional models cannot predict either cluster formation or reverse particle flow and hence the high particle loadings of circulating fluidized beds, without unjustifiable adjustment of the well-known drag relations.

Acknowledgment

This study was partially supported by National Science Foundation Grants Nos. CBT 851-3953 and CTS-8822740, which are industry-university cooperative programs with EXXON Research and Engineer-

ing Company. The authors thank Costas A. Coulaloglou for a helpful discussion.

The computations were made on the Cray X-MP computer at the National Center for Supercomputing Applications at the University of Illinois at Urbana-Champaign. The authors thank Michael Welge of NCSA for his help in making a computer-generated video display of the formation of clusters.

Notation

C_{ds} = drag coefficient of gas for single-particle system
D = riser diameter, m
d_p = diameter of particle, m
f_g = gas-wall friction coefficient
f_{gw} = gas-wall friction force, N/m^3
f_p, f_{sw} = solids-wall friction force, N/m^3
f_s = solids-wall friction coefficient
g = gravity acceleration, m/s^2
G = solids stress modulus, kg/m · s^2
$\bar{\bar{I}}$ = unit tensor
L = length of conveying line, m
L_p = particle mean free path, m
P = pressure, N/m^2
R = universal gas constant, kg · m^2/s^2 · kmol · K
Re = solid Reynolds number
Re_g = gas Reynolds number
T = temperature K
t = time, s
U_g, V_g = radial, axial gas velocities, m/s
U_s, V_s = radial, axial solids velocities, m/s
W_s = solids flux, kg/m^2 · s
x = axial coordinate, m

Greek letters

β = fluid-particle friction coefficient, kg/m^3 · s
∂t = time step, s
ϵ_g, ϵ = gas volume fraction
ϵ_s = solids volume fraction
ϵ_s = average solids volume fraction
ϕ_s = sphericity
μ_g, μ_s = gas, solids viscosity, kg/m · s
ρ_g, ρ_s = gas, solids denisty, kg/m^3
τ = solids stress, related to particle-particle pressure, N/m^2
$\bar{\bar{\tau}}_g, \bar{\bar{\tau}}_s$ = gas, solids microscopic viscous stress, Pa

Subscripts

g = gas
s = solids
w = wall

Superscripts

$\rightarrow$ = vector quantity
$\leftrightarrow$ = tensor quantity

Operators

$\nabla \cdot$ = divergence
∇ = gradient

Literature Cited

Abed, R., in *Fluidization,* D. Kunii, R. Toei, eds., Engineering Found., New York (1984).

Arastoopour H., and D. Gidaspow, "Analysis of IGT Pneumatic Conveying Data and Fast Fluidization Using a Thermodynamic Model," *Powder Technol.*, **22,** 77 (1979a).

———"Vertical Pneumatic Conveying Using Four Hydrodynamic Models," Ind. Eng. Chem. Fundam. **18,** 123 (1979b).

Bader, R., J. Findlay, and T. M. Knowlton, "Gas/Solid Flow Patterns in a 30.5 cm Diameter Circulating Fluidized Bed," 2d Int. Circulating Fluidized Bed Conf. March 14–18, Compiegne, France (1988).

Basu, P., and P. K. Nag, "An Investigation into Heat Transfer in Circulating Fluidized Beds," *Int. J. Heat Mass Transfer,* **30,** 11, 2399, (1987).

Bolton, L. W., and J. F. Davidson, "Recirculating of Particles in Fast Fluidized Risers," *Circulating Fluidized Bed Technology,* P. Basu, ed., Pergamon, Oxford (1988).

Bouillard, J. X., R. W. Lyczkowski, and D. Gidaspow, "Porosity Distributions in a Fluidized Bed with an Immersed Obstacle," *AIChE J.,* **35**(6), 908 (1989).

Capes, C., and K. Nakamura, "Vertical Pneumatic Conveying: An Experimental Study with Particles in The Intermediate and Turbulent Flow Regimes," *Canad. J. Chem. Eng.,* **51,** 31 (1973).

Ding, J., and D. Gidaspow, "A Bubbling Fluidization Model Using Kinetic Theory of Granular Flow," *AIChE J.,* **36,** 523 (1990).

Gajdos, L., and T. Bierl, "Studies in Support of Recirculating Bed Reactors for the Processing of Coal," Topical rept. for U.S. Dept. of Energy, Carnegie-Mellon Univ., Contract No. EX-76-c-01-2449 (1978).

Gidaspow, D., "A Thermodynamic Theory of Two-Phase Flow with Unequal Phase Velocities," *Proc. 1976 NATO Adv. Study Inst. Two-Phase Flows and Heat Transfer, Istanbul, Turkey, Aug. 16–27,* (1976).

———"Hydrodynamics of Fluidization and Heat Transfer: Supercomputer Modeling," *Appl. Mech. Rev.* **39**(1), 1 (1986).

Gidaspow, D., Y.P. Tsuo, and K.M. Luo, "Computed and Experimental Cluster Formation and Velocity Profiles in Circulating Fluidized Beds," *Fluidization IV,* Int. Fluidization Conf., Banff, Alberta, Canada, May (1989).

Grace, J. R., "Fluidized-Bed Hydrodynamics," *Handbook of Multiphase Systems,* G. Hetsoroni, ed., Ch. 8.1, McGraw-Hill, New York (1982).

Grace J. R., and J. Tuot, "A Theory for Cluster Formation in Vertically Conveyed Suspensions of Intermediate Density," *Trans. Inst. Chem. Eng.,* **57,** (1979).

Hartge, E., Y. Li, and J. Werther, "Analysis of the Local Structure of the Two-Phase Flow in a Fast Fluidized Bed," *Circulating Fluidized Bed Technology,* P. Basu, ed., Pergamon, Oxford (1986).

Horio, M., "Recent Data on the Scaling Law of Circulating Fluidized Beds," 17th IEA-AFBC Tech. Meet., Amsterdam (Nov. 1988).

IGT, Institute of Gas Technology, *Coal Conversion Systems Technical Data Book,* for U.S. Dept. Energy, Contract No. AC0181FE05157; available from Nat. Tech. Information Service (1982).

Jackson, R., "Hydrodynamic Stability of Fluid-Particle Systems," *Fluidization,* J. F. Davidson, R. Clift, D. Harrison, eds., Academic Press, 47 (1985).

Konno, H., and S. Saito, "Pneumatic Conveying of Solid through Straight Pipes," *J. Chem. Eng. Japan,* **2**(2), 211 (1969).

Leung, L. S., "The Ups and Downs of Gas-Solid Flow—A Review," *Fluidization,* J. R. Grace, J. M. Matsen, eds. Plenum, New York, London, 25 (1980); also in *Hydrodynamics of Gas-Solids Fluidization,* N. P., Chereminisoff, P. N. Chereminisoff, Gulf Pub. Corp., Houston (1984).

Luo K. M. "Dilute, Dense-Phase and Maximum Solid-Gas Transport," Ph.D. Thesis, Illinois Inst. Technology., Chicago (1987).

Lyczkowski, R. W., D. Gidaspow, C. W. Solbrig, and E. C. Hughes, "Characteristics and Stability Analyses of Transient One-Dimensional Two-Phase Flow Equations and Their Finite-Difference Approximations," *Nucl. Sci. Eng.* **66,** 378 (1978).

Matsen, J. M., "Mechanisms of Chocking and Entrainment," *Powder Technol.* **32,** 4 (1982).

———"The Rise and Fall of Recurrent Particles: Hydrodynamics of Circulation," *Circulating Fluidized Bed Technology,* P. Basu, ed., Pergamon, Oxford (1988).

Nakamura, K., and C. Capes, "Vertical Pneumatic Conveying: A Theoretical Study of Uniform and Annular Particle Flow Models," *Canad. J. Chem. Eng.,* **51,** 39 (1973).

Rhodes, M. J., and D. Geldart, "A Model for the Circulating Fluidized Bed," AIChE Ann. Meet., Miami Beach (1986).

Schnitzlein, M., and H. Weinstein, "Flow Characterization in High-Velocity Fluidization Beds Using Pressure Fluctuations," *Chem. Eng. Sci.,* **43**(10), 2605 (1988).

Sinclair, J. L., and R. Jackson, "Gas-Particle Flow in a Vertical Pipe with Particle-Particle Interactions," *AIChE J.,* **35**(9), 1473 (1989).

Soo, S. L., *Fluid Dynamics of Multiphase Systems,* Blaisdell, Waltham, MA (1967).
Squires, A. M., "The Story of Fluid Catalytic Cracking: The First Circulating Fluid Bed," *Circulating Fluidized Bed Technology* P. Basu, ed., Pergamon, Oxford (1986).
Squires, A. M., M. Kwauk, and A. A. Avidan, "Fluid Beds: At Last, Challenging Two Entrenched Practices," *Science,* **230**(4732), 1329 (1985).
Syamlal, M., "Multiphase Hydrodynamics of Gas-Solids Flow," Ph.D. Thesis, Illinois Inst. Technol., Chicago (1985).
Tsuo, Y. P., "Computation of Flow Regimes in Circulating Fluidized Beds," PhD Thesis, Illinois Inst. Technol., Chicago (1989).
Weinstein, H., M. Meller J. Shao, and R. J. Parisi, in *Fluidization and Fluid Particle Systems: Theories and Applications,* T. M. Knowlton, ed., *AIChE Symp. Ser.,* **80**(234) (1984).
Weinstein, H., M. Shao, M. Schnitzlein, and R. A. Graff, "Radial Variation in Void Fraction in a Fast Fluidized Bed," *Fluidization V, Proc. 5th Eng. Found. Conf. Fluidization, Elsinore, Denmark,* K. Østergaard, A. Sørensen, eds., 329 (1986).
Wu, R. L., J. R. Grace, C. J. Lim, and J. Chaouki, "Heat Transfer from a Circulating Fluidized Bed to Membrane Waterwall Surfaces," *AIChE J.,* **33**(11), 1888 (1987).
Yerushalmi, J., "High-Velocity Fluidized Bed," *Gas Fluidization Technology,* D. Geldart, ed., Wiley, Chichester, 155 (1986).
Yershalmi, J., and A. M. Squires, "The Phenomenon of Fast Fluidization," *AIChE Symp. Ser.,* **73,** 161 (1977).
Yerushalmi, J., D. H. Turner, and A. M. Squires, "The Fast Fluidized Bed," *Ind. Eng. Chem. Process Des. Dev., 15(1), 47 (1976).*
Youchou, L., and M. Kwauk, "The Dynamics of Fast Fluidization," *Fluidization, J. R. Grace,* J. M. Matsen, eds., Plenum, New York (1980).

Appendix A. Characteristic Analysis

The characteristic directions for the propagation of the gas and the solids have been examined for the one-dimension inviscid case. In the nonconservative form, the continuity and the momentum equations for gas-solids flow are as follows,

$$\overline{\mathbf{A}}\begin{pmatrix} \frac{\partial \epsilon_g}{\partial t} \\ \frac{\partial P}{\partial t} \\ \frac{\partial V_g}{\partial t} \\ \frac{\partial V_s}{\partial t} \end{pmatrix} + \overline{\mathbf{B}}\begin{pmatrix} \frac{\partial \epsilon_g}{\partial x} \\ \frac{\partial P}{\partial x} \\ \frac{\partial V_g}{\partial x} \\ \frac{\partial V_s}{\partial x} \end{pmatrix} = \overline{\mathbf{C}} \tag{A1}$$

where

$$\overline{\mathbf{A}} = \begin{pmatrix} \rho_g & \frac{\epsilon_g}{C^2} & 0 & 0 \\ \rho_s & 0 & 0 & 0 \\ 0 & 0 & \rho_g \epsilon_g & 0 \\ 0 & 0 & 0 & \rho_s \epsilon_s \end{pmatrix} \tag{A2}$$

and

$$\overline{\mathbf{B}} = \begin{pmatrix} \rho_g V_g & \frac{\epsilon_g V_g}{C^2} & \rho_g \epsilon_g & 0 \\ \rho_s V_s & 0 & 0 & \rho_s \epsilon_s \\ 0 & 1 & \epsilon_g \rho_g V_g & 0 \\ -G & 0 & 0 & \epsilon_s \rho_s V_s \end{pmatrix} \tag{A3}$$

and

$$\overline{\mathbf{C}} = \begin{pmatrix} 0 \\ 0 \\ f_{gs} + f_{gw} + \epsilon_g \rho_g g \\ f_{sg} + f_{sw} + \epsilon_s \rho_s g \end{pmatrix} \tag{A4}$$

where

$$C = \sqrt{\left(\frac{\partial P}{\partial \rho_g}\right)_T}$$

The characteristic determinant is

$$\begin{vmatrix} V_s - \lambda & 0 & 0 & -\epsilon_s \\ \frac{\rho_g C^2}{\epsilon_g}(V_g - V_s) & V_g - \lambda & \rho_g C^2 & \frac{\epsilon_s \rho_g C^2}{\epsilon_g} \\ 0 & \frac{1}{\rho_g \epsilon_g} & V_g - \lambda & 0 \\ -\frac{G}{\epsilon_s \rho_s} & 0 & 0 & V_s - \lambda \end{vmatrix} = 0 \tag{A5}$$

The characteristic roots, λ_i, of the above determinant are

$$\lambda_{1,2} = V_g \pm \sqrt{\frac{C^2}{\epsilon_g}} \tag{A6}$$

and

$$\lambda_{3,4} = V_s \pm \sqrt{\frac{G}{\rho_s}} \tag{A7}$$

Since $C^2/\epsilon_g > 0$, and $G/\rho_s > 0$, this equation set has real and distinct characteristics. Hence the system is hyperbolic. The problem is well posed as an initial-value problem (Lyczkowski et al., 1978).

The characteristic directions also determine where the boundary conditions must be prescribed for a well-posed problem. Equation A6 shows that information about the gas must be prescribed at the inlet and at the exit, since the characteristic directions are positive and negative due to the large value of C. Although the form for the solids, as shown by Eq. A7, is similar to that for the gas, the value of G/ρ_s is small. Its square root is of the order of 1 m/s for dense flow, for a volume fraction of solids of about 0.6. It is very low for dilute flow. Hence, normally the characteristic directions for the solids are both positive. For small values of G, the characteristics are nearly equal. The particles essentially move with their own velocity, with the wave effect negligible. Hence in a CFB where there is reverse flow, a boundary condition for the solids must be prescribed at the top of the pipe.

In a strict sense, this analysis is not applicable to viscous flow. However, it is known that the viscous terms are a correction, since the viscous dissipations, both in the gas and the solid

phases, are much smaller than the dissipation, due to the drag between the particles and the gas. Hence an inviscid analysis provides a useful guide. The introduction of a bend at the top of the pipe provided a valid boundary condition for the solid in the downflow region, whenever it existed. The normal component of the solid velocity was zero. Such a situation corresponds to the experimental conditions and to industrial practice. The disadvantage of this approach is that a slice of the pipe had to be studied in two dimensions, since axial symmetry could no longer be used.

Appendix B. One-Dimensional Equations of Change

Gas continuity equation

$$\frac{\partial(\rho_g \epsilon_g)}{\partial t} + \frac{\partial(\rho_g \epsilon_g U_g)}{\partial x} = 0 \tag{B1}$$

Solid continuity equation

$$\frac{\partial(\rho_s \epsilon_s)}{\partial t} + \frac{\partial(\rho_s \epsilon_s U_s)}{\partial x} = 0 \tag{B2}$$

Gas momentum equation

$$\frac{\partial(\rho_g \epsilon_g U_g)}{\partial t} + \frac{\partial(\rho_g \epsilon_g U_g U_g)}{\partial x} = -\frac{\partial P}{\partial x} + \beta(U_s - U_g) + \frac{2 f_g \epsilon_g \rho_g U_g^2}{D} + \epsilon_g \rho_g g \tag{B3}$$

Solids momentum equation

$$\frac{\partial(\rho_s \epsilon_s U_s)}{\partial t} + \frac{\partial(\rho_s \epsilon_s U_s U_s)}{\partial x} = \beta(U_g - U_s) - G\frac{\partial \epsilon_s}{\partial x} + \frac{2 f_s \epsilon_s \rho_s U_s^2}{D} + \epsilon_s \rho_s g \tag{B4}$$

Friction factors:

Modified Hagen-Poiseuille expression

$$f_g = \frac{16}{Re_g} \quad \text{for} \quad Re_g \le 2{,}100 \tag{B5}$$

$$f_g = \frac{0.0791}{Re_g^{0.25}} \quad \text{for} \quad 2{,}100 < Re_g \le 100{,}000 \tag{B6}$$

$$\frac{1}{\sqrt{f_g}} = 2 \log (Re_g \sqrt{f_g}) - 0.8 \quad \text{for} \quad Re_g > 100{,}000 \tag{B7}$$

where

$$Re_g = \frac{D U_g \rho_g \epsilon_g}{\mu_g}$$

Konno's correlation

$$f_s = 0.0025 U_s^{-1} \tag{B8}$$

Manuscript received Apr. 21, 1989, and revision received Apr. 4, 1990.